Online First: This article has been peer-reviewed and accepted, and is awaiting editing or assignment to a final issue, but it is citable using its DOI.

FORUM GEOGRAFI
ISSN: 0852-0682 | E-ISSN: 2460-3945

HTTPS://JOURNALS.UMS.AC.ID/INDEX.PHP/FG/

Research article

High-Resolution Bathymetry of the Southern Pantar Strait Reveals the Deep Cold-Water Source of Extreme Upwelling off Alor Kecil, Indonesia

Anindya Wirasatriya[1,2*], Gentio Harsono[3,4], Dwi Haryanti[5], R. Dwi Susanto[6], Lilik Maslukah[1], Yusuf Jati Wijaya[1,2], Ni Kadek Dita Cahyani[7,8], Rizki Taqwa Putranto[1,2], Riandi Teguh Widiyandono[2], Faisal Hamzah[9], Iis Triyulianti[10], Muhammad Helmi[1], Alexander Yosep Elake[11], Gede Iwan Setiabudi[12], Deirus Rizki Khair[3], Mohan Syafaat[3], Danar Judas Pratama[3], Yohanes Theo Medhika[3], Darminto[3], Agung Setyo Sasongko[13], Azis Rifai[1], Dwiyoga Nugroho[9], Jahved Ferianto Maro[14]

[1] Department of Oceanography, Faculty of Fisheries and Marine Science, Diponegoro University, Semarang 50275, Indonesia, [2] Atmosphere-Ocean Interaction (Blue) Laboratory, Faculty of Fisheries and Marine Science, Diponegoro University, Semarang 50275, Indonesia, [3] Hydro-Oceanographic Center, Indonesian Navy, Jl. Pantai Kuta V No. 1 Jakarta, Indonesia, [4] Faculty of Defense Strategy, Republic of Indonesia Defense University, Indonesia, [5] Department of Marine Science, Faculty of Fisheries and Marine Science, Diponegoro University, Semarang 50275, Indonesia, [6] Department of Atmospheric and Oceanic Science, University of Maryland, College Park, MD 20742, USA, [7] Diponegoro Biodiversity Project (DBP) Laboratory, Diponegoro University, Semarang 50275, Indonesia, [8] Department of Biology, Faculty of Science and Mathematics, Diponegoro University, Semarang 50275, Indonesia, [9] Research Center for Oceanology, National Research and Innovation Agency, Jakarta, Indonesia, [10] Research Center for Deep Sea, National Research and Innovation Agency, Jakarta, Indonesia, [11] Department of Physics, Faculty of Science and Technology, Universitas Pattimura, Ambon, Indonesia, [12] Department of Aquaculture, Universitas Pendidikan Ganesha, Singaraja, Bali, Indonesia, [13] Department of Marine and Fisheries Education, Universitas Pendidikan Indonesia, Bandung, Indonesia, [14] Dept. of Fisheries, Faculty of Agriculture and Fisheries, Universitas Tribuana Kalabahi, Alor, Indonesia.

[*)] Correspondence: anindyawirasatriya@lecturer.undip.ac.id

Citation:
Wirasatriya, A., Harsono, G., Haryanti, D., Susanto, R. D., Maslukah, L., Wijaya, J., Cahyani, N. K. D., Putranto, R. T., Widiyandono, R. T., Hamzah, F., Triyulianti, I., Helmi, M., Elake, A. Y., Setiabudi, G. I., Khair, D. R., Syafaat, M., Pratama, D. J., Medhika, Y. T., Darminto, Sasongko, A. S., Rifai, A., Nugroho, D & Maro, J. F. (2026). High-Resolution Bathymetry of the Southern Pantar Strait Reveals the Deep Cold-Water Source of Extreme Upwelling off Alor Kecil, Indonesia. Forum Geografi. 40(3), 407-420.

Article history:
Received: 19 January 2026
Revised: 3 July 2026
Accepted: 13 July 2026
Published: 15 July 2026

Abstract

An extreme upwelling event (EUE) off Alor Kecil (central Pantar Strait, Indonesia) can cause sea-surface temperature (SST) to drop by >10 °C within hours, indicating rising cold water from the deep basin. The EUE occurs along the Mulut Kumbang Strait, a narrow channel 300 m wide and 900 m long. Understanding the water-mass origin of the EUE may provide insights into the mechanism of EUE generation. Prior eDNA analyses suggested a deep-ocean source (Savu Sea Basin) based on the detection of bathypelagic fish genetic materials at the Mulut Kumbang Strait during the EUE, which indicates that the water-mass origin of the EUE may come from a depth of more than 1,000 m. To confirm the source of the cold-water mass, we present a multibeam echosounder (MBES) bathymetric survey to observe the detailed bottom morphology of the Pantar Strait. We also provide Conductivity Temperature Depth (CTD) data from five stations in the Pantar Strait, which measure the vertical profile of temperature. We identified five basins in the southern Pantar Strait that are likely the sources of the cold-water mass originating in the Mulut Kumbang Strait. The first basin is situated south of the Mulut Kumbang Strait and has a depth of approximately 150 m. The second, third, and fourth basins are aligned further south, with depths of ~350, ~400, and ~600 m, respectively. The deepest and largest basin is located at the southernmost point of the Pantar Strait, adjacent to the Savu Sea, and reaches a maximum depth of 1,060 m. The area of the basin that exceeds 1,000 m in depth covers 4.75 km^2. CTD data confirm that temperatures below 10 °C are found at depths greater than 400 m. We infer that the largest and deepest basin at the southern end of the Pantar Strait is a plausible source reservoir for the cold-water mass during the EUE, which is potentially connected to the Mulut Kumbang Strait via a tapered channel.

Keywords: extreme upwelling; sea surface temperature; multibeam bathymetry; seafloor topography; bottom topography; cold-water mass; Pantar Strait; Alor Island.

1. Introduction

Upwelling involves lifting water masses from deep water columns to the surface over an extended period (several days to weeks), allowing them to rise over 100 m (Kampf and Chapman, 2016). Coastal upwelling is driven by surface winds along the coast that produce offshore Ekman Transport, bringing cold-water masses to the surface (Moore II *et al.*, 2003; Susanto *et al.*, 2006; Kämpf 2015; Ningsih *et al.*, 2013; Wirasatriya *et al.*, 2019a,b, 2020, 2021; Setiawan and Kawamura 2011; Setiawan and Habibi, 2011; Setiawan *et al.*, 2019, 2020; García-Reyes and Largier, 2010; Narayan *et al.*, 2010). While typical coastal upwelling leads to sea surface temperature (SST) drops of 2–4 °C, an extreme upwelling event (EUE) in Alor Kecil results in a remarkable SST decrease of more than 10 °C, making it a unique phenomenon (Wirasatriya *et al.*, 2023, 2025a, b; Astuti *et al.*, 2025; Putranto *et al.*, 2025). Continuous observations indicate SST minima as low as 12 °C during an EUE, which is unusually cold for tropical seas (e.g., Saraswat *et al.*, 2005; Chen *et al.*, 2016; Du *et al.*, 2008; Wang *et al.*, 2012; Weingner and Weisberg, 1991; Delman *et al.*, 2016; Sie *et al.*, 2025; Wirasatriya *et al.*, 2021). In addition, the temperature drop during the EUE in Alor Kecil is not comparable to the extreme upwelling in Monterey Bay, California, as observed by Harvey *et al.*, (2021).

Unlike typical coastal upwelling events that are primarily driven by wind forcing, the upwelling observed in the Mulut Kumbang Strait is tide-driven and is distinguished by its occurrence in synchrony with the lunar cycle during spring tides. This phenomenon manifests monthly between August and November, with two discrete upwelling events per day, each lasting approximately one hour and spanning a total duration of 1–3 days during the peak spring tide periods. The spatial confinement of this upwelling to the narrow Mulut Kumbang Strait, a channel approximately 300 m wide and 900 m long between Alor Kecil Village and Kepa Island (Figure 1), underscores the strong topographic control of the tidal dynamics that incite this process. Observations have revealed that flood currents during spring tides advect colder, nutrient-rich waters into the strait, whereas ebb currents subsequently export these waters out of the channel into adjacent marine areas, particularly at the strait's mouth (Wirasatriya *et al.,* 2023).

Tide-driven upwelling, as observed in the Mulut Kumbang Strait, is conceptually distinct from wind-driven coastal upwelling and involves complex hydrodynamic interactions in semi-enclosed or constricted straits where tidal currents are intensified by geometric funneling and bathymetric features. Similar tidally amplified upwelling has been documented in narrow straits and peripheral basins where tidal wave amplification and resonance effects induce strong tidal currents capable of entraining and transporting deeper, cooler waters upward and into coastal or embayment zones (Longhitano, 2010; Reynaud and Dalrymple, 2011).

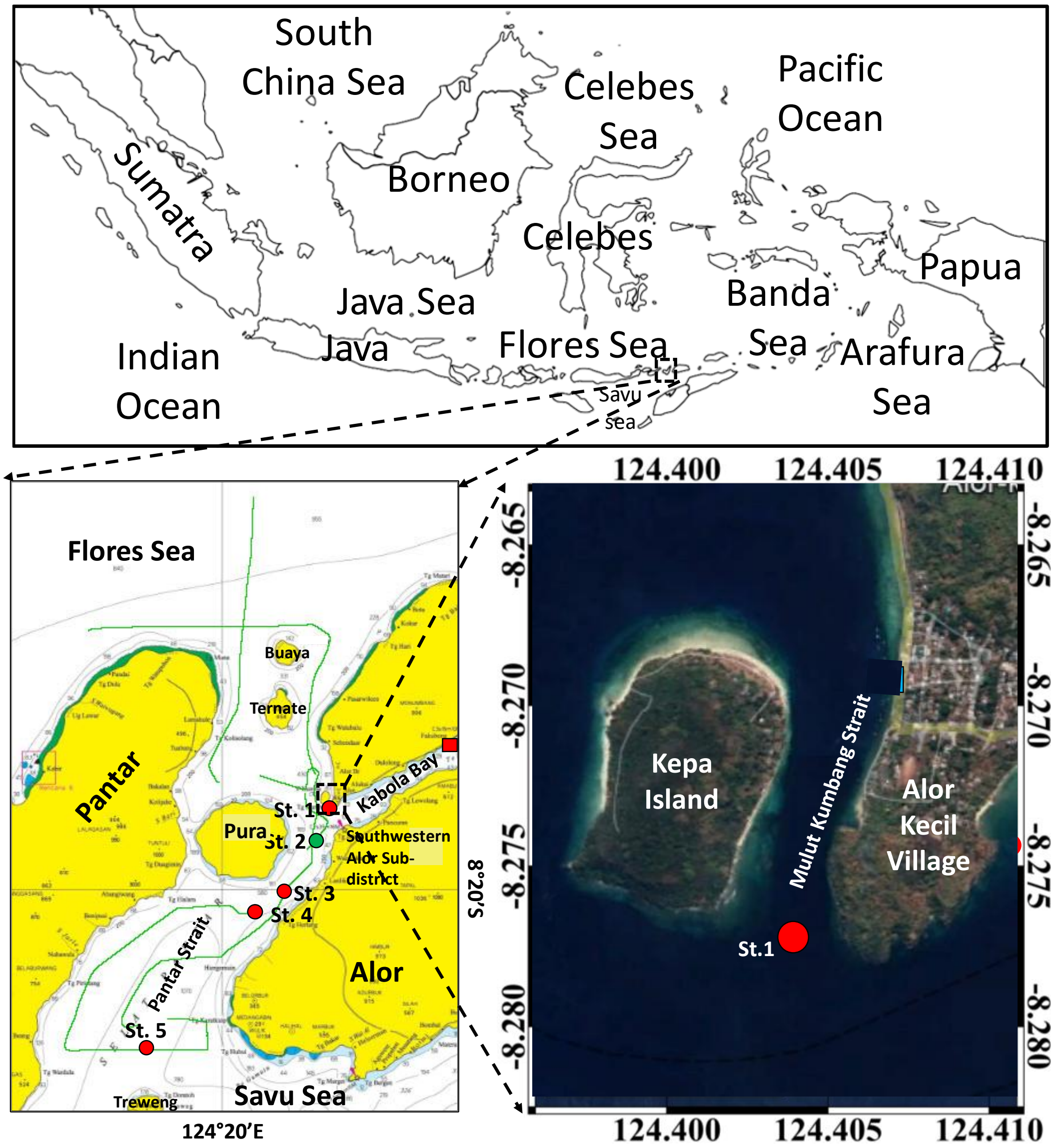

Figure 1. Map of the Pantar Strait Study Area.

The MBES Track Onboard KRI SPICA 934 Is Denoted by the Green Line. Red and Green Dots Represent the Position of CTD Casts by KRI SPICA 934 and by Wirasatriya *et al.*, (2023), Respectively. The Red Box Is the Tidal Station at Kalabahi Operated by the Geospatial Information Agency (BIG) of Indonesia.

The timing of these upwelling events aligning with spring tides is consistent with the modulation of tidal energy and currents by the lunar cycle, wherein the spring neap cycle generates substantial fortnightly fluctuations in tidal current strength and vertical mixing processes. Such tidal modulation can strongly influence the biogeochemical properties, stratification, and ecosystem dynamics of coastal waters. For instance, spring tides intensify tidal currents and enhance the vertical mixing and upwelling of nutrient-rich colder water, whereas neap tides correspond to weaker currents and reduced upwelling intensities (Sharples, 2007; Xing *et al.,* 2021; Susanto and Ray, 2022).

Using a thermal infrared sensor mounted on an unmanned aerial vehicle (UAV), Wirasatriya *et al.,* (2025a) indicated the interaction between tidal currents and Indonesian Throughflow (ITF), which regulates the generation and decay of EUE along the Mulut Kumbang Strait. The northward flood current must be sufficiently strong to push the ITF, which moves southward to generate the EUE. Conversely, the EUE decays when the southward ebb current collides with the ITF, pushing the cold-water mass out of the Mulut Kumbang Strait.

Using single beam echosounder (SBES), Wirasatriya *et al.,* (2023) indicated that the source of cold-water in the EUE is from the deep basin (~300 m) located between Pura Island and the Southwestern Alor sub-district based on their conductivity temperature depth (CTD) observation, and the temperature at more than 270 m depth is around 10 °C. SBES bathymetry and CTD profiles suggested a 300 m basin connected to the Mulut Kumbang Strait by a channel that could focus on the tidal transport of cold water without dispersing into surrounding areas. However, the analysis of eDNA during EUE by Astuti et al. (2025) revealed that the source of the cold-water mass may come further south from the Savu Sea Basin, as they found genetic materials from the deep-sea fish community in the bathypelagic zone (1,000–4,000 m). While previous studies have identified potential sources of cold-water masses, the use of SBES and eDNA has limitations, particularly in terms of spatial resolution and depth coverage. Thus, these indications need to be examined further by conducting a wider area survey, increasing the density of bathymetry observations and including more CTD sampling stations to confirm the cold-water mass origin of the EUE.

To gain a clearer understanding of the origins of cold-water masses, this study used multibeam echosounder (MBES) data to create high-resolution comprehensive seabed maps of the Pantar Strait. Unlike SBES, which measures depth at a single point, MBES allows us to map the seabed morphology across a broader area, providing more precise and comprehensive seabed mapping in each pass (Khomsin *et al.,* 2021). Furthermore, we also provide CTD data from five stations that can detail a vertical temperature profile to examine the possibility of a cold-water mass origin of the EUE in the Pantar Strait.

2. Methods

2.1. Study Area

The field survey was conducted during the Jala Citra 3–2023 Flores Expedition, which passed through the Pantar Strait on 4–5 April and May 18, 2023. This expedition was a marine research activity with the theme "Uncovering Ocean Floor Features and Characteristics of the Flores Sea Water Column for Navigation Safety, Defense, and Sustainable Marine Development." The research cruise was organized by the Hydro-Oceanography Center, Indonesian Navy, in collaboration with researchers from relevant Ministries/Agencies, Universities, and professionals, and private parties engaged in marine surveying and mapping. One of the targeted areas of the Jala Citra Expedition was Pantar Strait Figure 1.

2.2. Instrument

To investigate the origin of the EUE cold-water mass, we used the MBES Kongsberg EM 302 and CTD Valeport Midas SVX2 onboard the Research Vessel (RV) KRI SPICA 934 operated by the Center for Hydro-Oceanography Indonesian Navy. For navigation, the KRI SPICA 934 was equipped with a GNSS fUGRO SeaSTAR 3610 for accurate georeferencing.

With a 30 kHz frequency and 0.5° to 4° beam width, the depth range (swath width) of MBES EM 302 is from 10 m to 7,000 m (up to 5.5 times water depth / 8 km). The MBES 302 system has up to 288 beams / 432 soundings per swath with pointing angles that can automatically be adjusted according to the achievable coverage. In the present study, the equiangular beam spacing of the MBES EM 302 was set with a beam width and angular coverage of 1° and 12°–70°, respectively. The vessel speed was maintained at 4–7 knots during the measurement from 4–5 April 2023. The MBES paths in the Pantar Strait are parallel to the coastline, as shown in Figure 1, with a total path length of 105,030 m. The cross path was not conducted for safety reasons because the narrow strait and strong current in the Pantar Strait restricted vessel maneuvers.

The specifications of the CTD Midas SVX2 are listed in Table 1. The geographic location of the CTD deployment, with one cast per station, is shown in Figure 1 and Table 2. The tidal conditions of the CTD casts are shown in Figure 2. In addition, we used the CTD of Wirasatriya *et al.,* (2023), obtained from the CTD Sea-Bird Electronic SBE 37SMP (Station 2).

Table 1. Specification of CTD Midas SVX2.

Variable	Range	Resolution	Accuracy
Sound velocity	1375–1900m/s	0.001m/s	±0.02m/s
Conductivity	0 to 80 mS/cm	0.003mS/cm	±0.01mS/cm
Temperature	-5°C to +35°C	0.005°C	±0.01°C
Pressure	10, 50, 100, 300 or 600bar	0.001% range	±0.01% range

Table 2. Geographic position and depth of CTD station.

Station	Date Time (WITA)	Longitude (°E)	Latitude (°S)	Water Depth (m)
1	5/18/23 01:10	124.404	-8.278	74.47
2	6/15/22 15:00	124.395	-8.308	333.43
3	4/4/23 16:53	124.372	-8.340	445.991
4	5/18/23 08:00	124.351	-8.348	580.835
5	4/4/23 20:09	124.294	-8.436	1,059.138

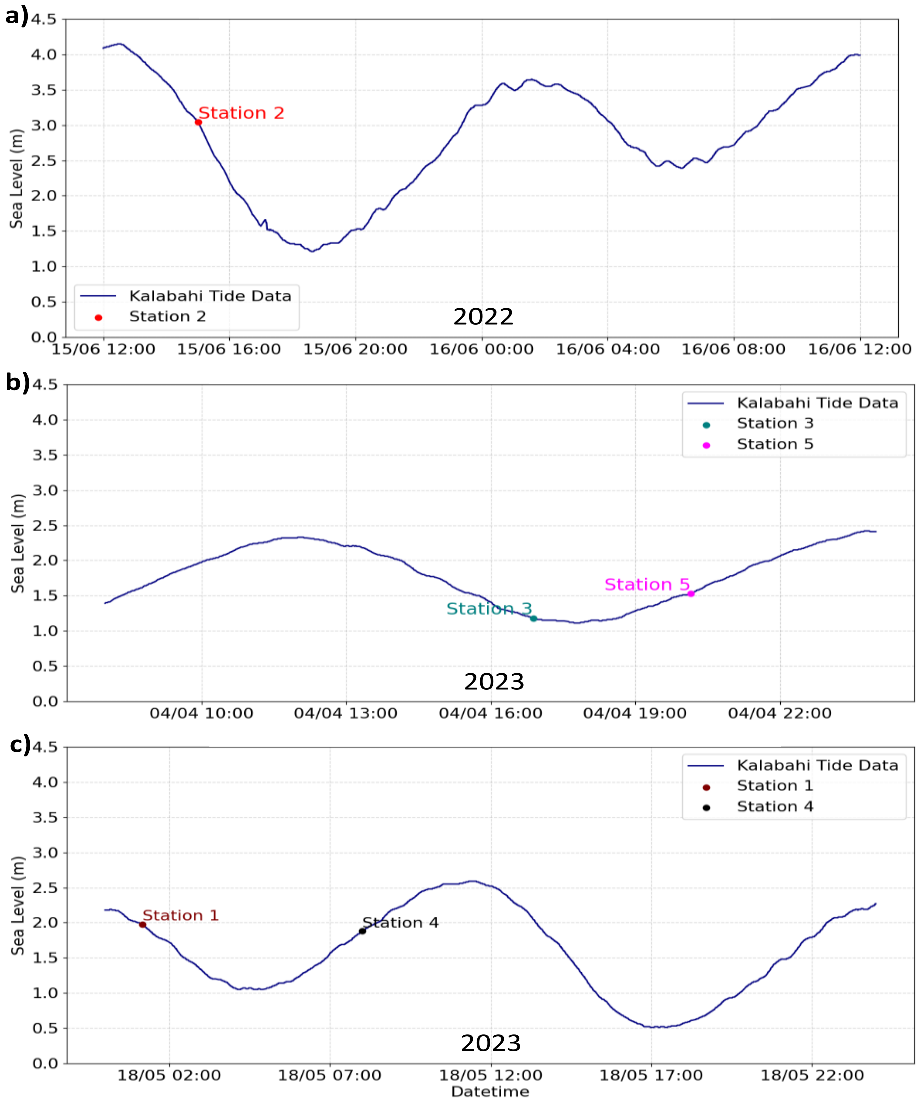

Figure 2. Tidal Condition During the CTD Deployment in the Pantar Strait. Tide Data Are Provided by BIG at Kalabahi Station Figure 1.

2.3. MBES and CTD Data Analysis

2.3.1. MBES Data Analysis

The MBES data were processed using CARIS HIPS and SIPS software licensed to the Hydro-Oceanography Center of the Indonesian Navy. CARIS HIPS and SIPS are professional hydrographic data-processing software suites developed by Teledyne CARIS. This is widely considered the industry standard for processing sonar and lidar data collected during maritime surveys. The acronym HIPS (SIPS) stands for Hydrographic Information Processing System (Sonar Information Processing System) that focuses on bathymetry/depth data (seafloor imagery and backscatter). Data processing in CARIS HIPS and SHIPS follows the Combined Uncertainty and Bathymetry Estimator) (CUBE) workflow (Canadian Hydrographic Service, 2012). The MBES data analysis was divided into three steps: correction and calibration, data cleaning, and gridding and visualization Figure 3.

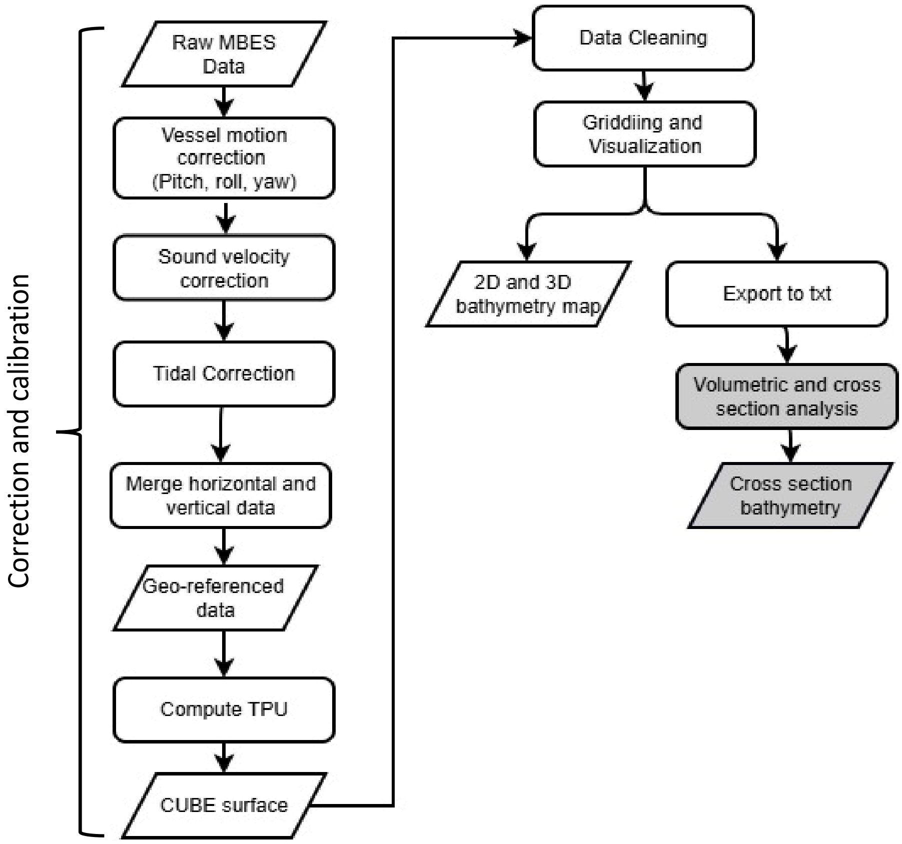

Figure 3. Flowchart of MBES Data Analysis. White and Gray Rectangles Are Processed Using CARIS HIPS and SIPS and QGIS, Respectively.

1. Correction and calibration

Vessel motion corrections were applied to the raw depth data from the MBES by adjusting the vessel pitch, roll, and yaw using motion sensors and GPS data. The results of the MBES EM 302 KRI Spica-934 patch test were obtained at depth of 124 m–3000 m Table 3. Subsequently, the data were calibrated to reduce the errors and ensure accuracy. The first calibration step was sound velocity correction, which is essential for accurate depth measurements. The speed of sound in water is influenced by the temperature, salinity, and pressure, and variations in these factors can lead to significant measurement errors. Four CTD casts were used to profile the water column and to correct for these variations. The second calibration was a tidal correction using tidal prediction, which was validated with a tide gauge at the Kalabahi Station to ensure that depth measurements were corrected relative to the mean lower low-water level. Subsequently, the horizontal (position) and vertical (depth) data were merged to produce georeferenced data.

The horizontal and vertical total propagated uncertainties (TPUs) were determined according to established procedures, including the EM 302 KRI Spica offset calculation and patch test. Analysis of the post TPU horizontal calculation values derived from the sounding results in this area indicates that the parameters influencing the sounding results are as follows: sonar 50%, roll 18%, pitch 17%, heading 9%, GPS 3%, IMU Timing 2%, and other 1%. Similarly, the post TPU vertical values from the sounding results suggest that the parameters affecting the results were sonar (angle) 38%, sonar (range) 22%, sound velocity 21%, roll 14%, tide 3%, and others 3%. The calibrated merged data were used to produce the CUBE surface. Quality control (QC) of the CUBE surface was a transducer performance test to correct any misalignment of the echosounder transducers to ensure accurate beam angles. The purpose of the performance test was to determine the best MBES swath angle for use in sounding activities. A performance test of the EM 302 KRI Spica-934 was carried out on a relatively flat bottom surface. The results of the performance tests at depths of 650–850 m with various beam angles are shown in Figure 4.

Table 3. Patch Test Correction on EM 302 KRI SPICA 934.

Date	System	Pitch (°)	Roll (S)	Yaw (Heading)	Latency (Sec)
6 April 2023	302	0	0	74.47	0.1

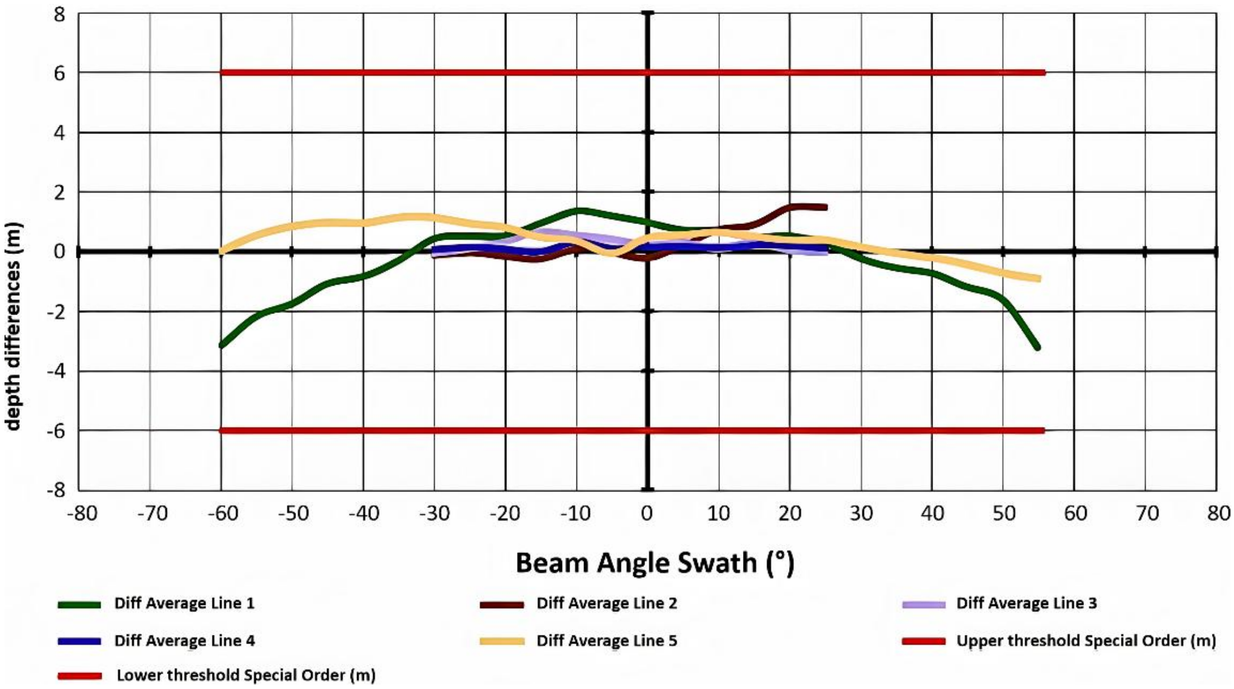

Figure 4. Vertical Uncertainty Validation That Explains the Difference Between Soundings and the Reference Surface Relative to the Beam Angle in the Swath Opening.

2. Data cleaning

After data calibration, data cleaning was performed using a high-pass filter to remove high-frequency noise from the vessel movement and other sources. Furthermore, spurious data points such as spikes that do not represent actual seabed features were manually identified as outliers and removed by visual inspection of the swath data.

3. Gridding and visualization

Finally, gridded data were obtained by interpolating the missing data points within the grid to create a continuous surface and merged data from multiple passes over the same area to improve coverage and accuracy. The final grid resolution of the bathymetry map was 30 m, and the bathymetry map was visualized in 2D and 3D formats. Volumetric and cross-sectional analyses were performed using QGIS 4.0.

2.3.2. CTD Data Analysis

Raw CTD data were processed using DataLog X2, a license-free application, to extract vertical sound velocity, temperature, conductivity, and salinity data. The vertical temperature profile was visualized using Ocean Data View (ODV) software. ODV is an open-source computer program used for interactive exploration, analysis, and visualization of oceanographic and other geo-referenced data. The vertical profiles of temperature data from the five CTD stations were interpolated using the Data-Interpolating Variational Analysis (DIVA) method embedded in ODV to obtain the vertical temperature distribution along the Pantar Strait.

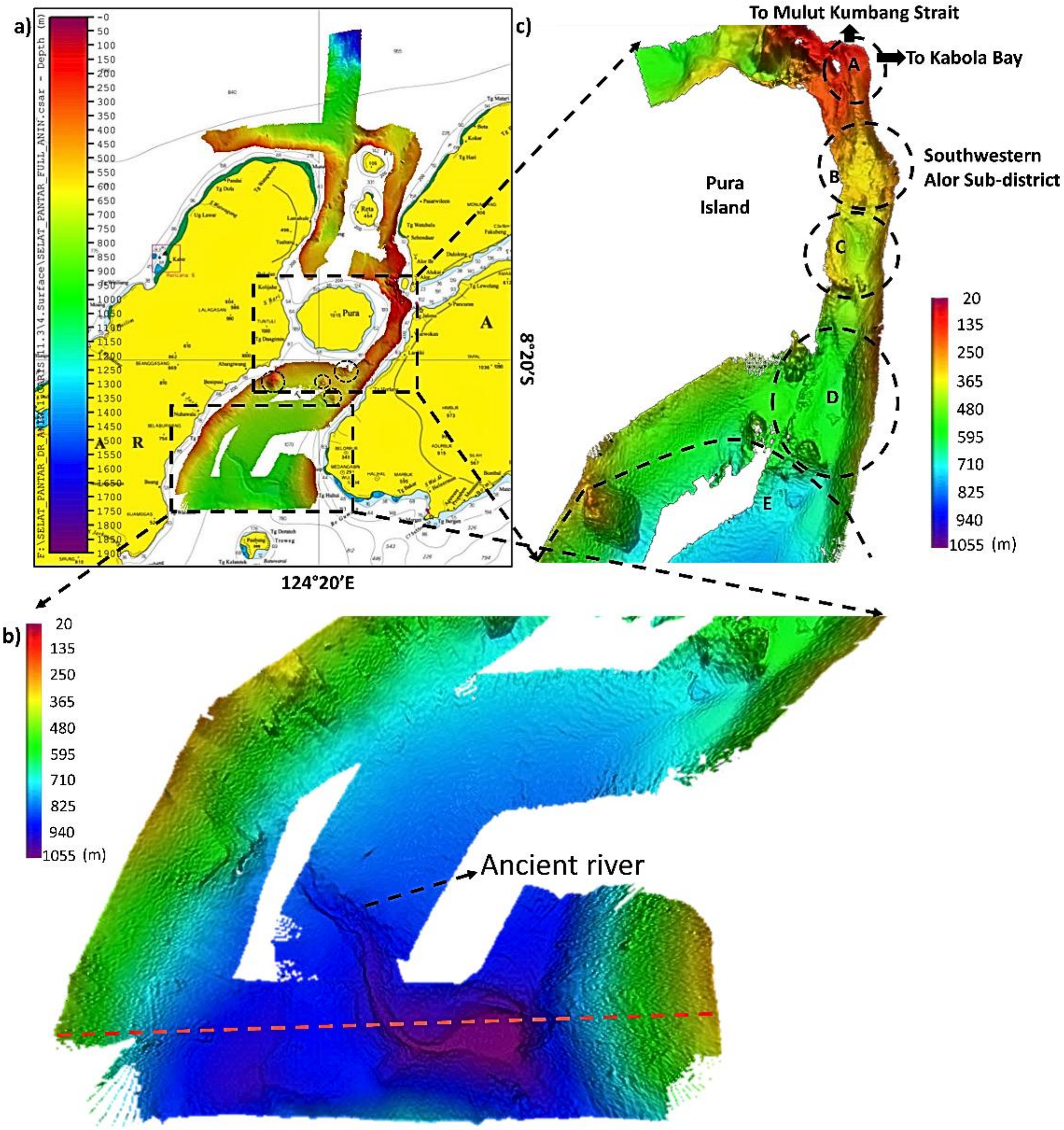

Figure 5. Bottom Topography Map of Pantar Strait Observed by MBES for (a) the Whole MBES Track, (b) Southern Part of Pantar Strait, and (c) Middle Part of Pantar Strait.

Black circles in (a) denote the detection of four submarine ridges at the southern part of Pura Island, while the black circles in (c) are the five basins (i.e., Basins A, B, C, D, and E) along the channel that connects the Mulut Kumbang Strait to the deepest basin at the southern part of Pantar Strait. The dashed red line in (b) denotes the cross-section line of bathymetry as shown in Figure 5.

3. Results and Discussion

3.1. Bottom Topography of Pantar Strait

The bottom topography of the Pantar Strait was determined using bathymetry data obtained from the MBES survey on 4-5 April 2023, spanning from the Flores Sea to the southern tip of the Pantar Strait Figure 5a. The deepest part of the bathymetric survey was located in the Flores Sea, reaching a depth of 1,800 m. In the northern part of Pura Island in the Pantar Strait, the seabed is generally shallow, with a depth of less than 400 m. The southwestern part of Ternate Island features a seabed depth of up to 650 m, while the southern part of Pura Island is dominated by a deep bowl-like basin, with a wide plain reaching depths of approximately 800 m.

To investigate the source and propagation path of the cold-water mass of the EUE, the analysis focused on the middle of the Pantar Strait in the eastern part of Pura Island Figure 5c. Taking advantage of high-resolution bathymetry from the MBES, five basins (A, B, C, D, and E) were observed along the channel that connects the Mulut Kumbang Strait to the deepest basin in the southern part of the Pantar Strait. Basins A–D have characteristic depths of 150, 350, 400, and

600 m. Basin E is the deepest and largest basin in the southern part of the Pantar Strait. Four oceanic ridges were identified at the northern tip of this basin, as indicated by the black circles in Fig. 5a. In contrast, at the southern tip, the deepest part of this basin was observed, reaching more than 1,000 m Figure 5b. Interestingly, a river-like meandering channel spanning from the continental slope and flowing southeastward to the deepest basin was observed. This indicated the existence of an ancient geological process that created the channel. However, this feature is beyond the scope of this study and is left for future research.

To obtain more detailed features of these basins, a three-dimensional (3D) model was generated along the channel, as shown in Figure 6. Figure 6 shows that the basins have coarse surfaces with ridges bordering each basin. However, a channel was clearly observed spanning from the Mulut Kumbang Strait to Basin E. From Basin E, this channel tapered to the Mulut Kumbang Strait. The tapered shape of the channel leading from Basin E to the Mulut Kumbang Strait suggests that it could act as a funnel, concentrating and directing the cold-water mass toward the strait. This narrowing of the channel may help explain the extreme nature of the upwelling event by facilitating the concentrated flow of cold water into the strait. Furthermore, a tall ridge is observed on the right side of Basin A in the western part of the mouth of the Mulut Kumbang Strait. This ridge has a steep slope at a height of 300 m from its base, which may hamper water masses spilling out of the channel.

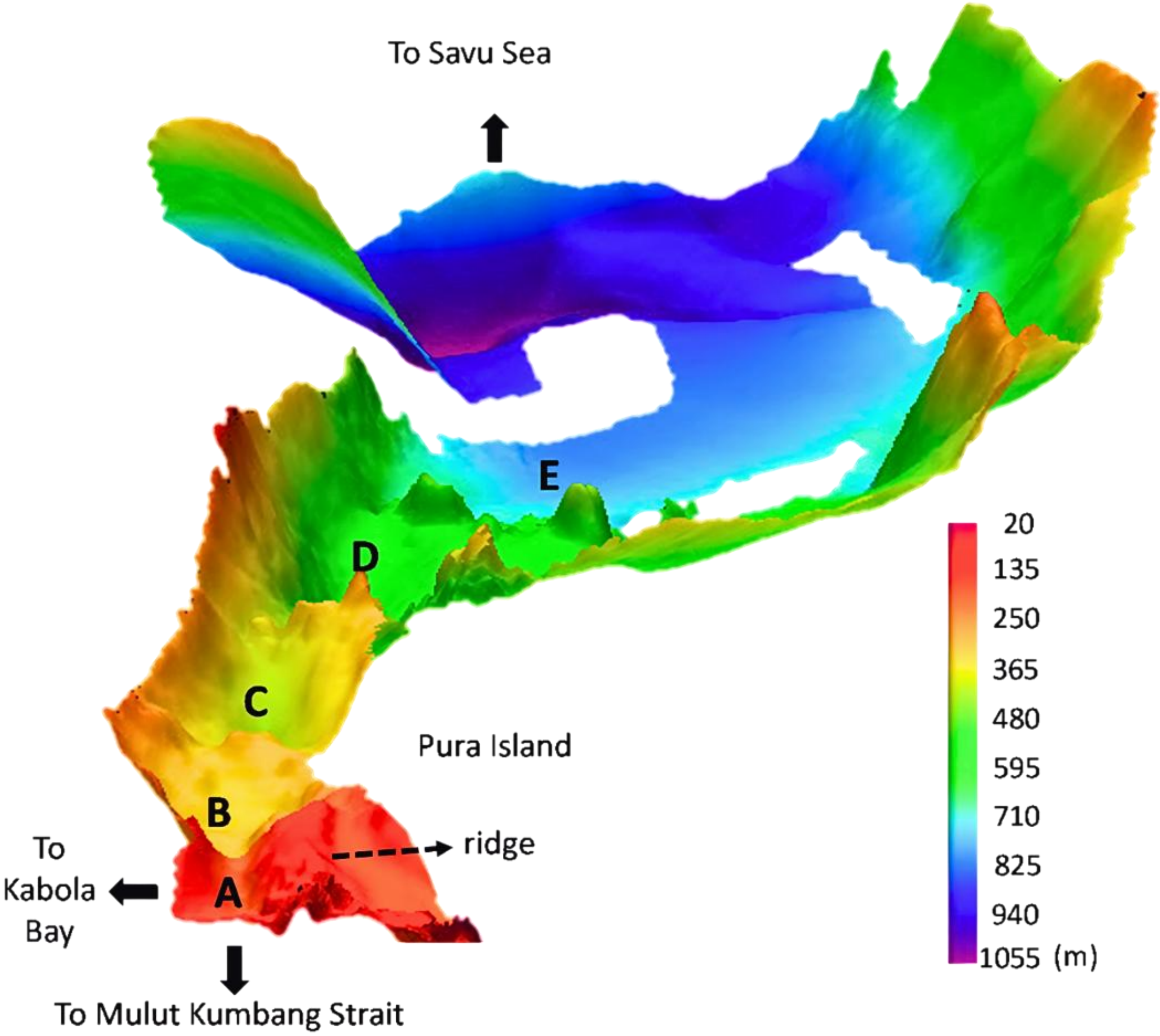

Figure 6. Three-Dimensional Model of Bathymetry Along the Channel That Connects the Mulut Kumbang Strait to the Deepest Basin at the Southern Part of Pantar Strait.

The Observed Five Basins Along the Southern Pantar Strait Are Marked by A, B, C, D, and E. The high-resolution bathymetry map processed from MBES managed to reveal the area of Basin E, which exceeds 1,000 m in depth, covers 4.75 km² Figure 7a, and has a volume of 150.96 × 10^6 m^3. The cross-section of the bathymetry in the deepest basin shows that the deepest basin reaches 1,060 m Figure 7b.

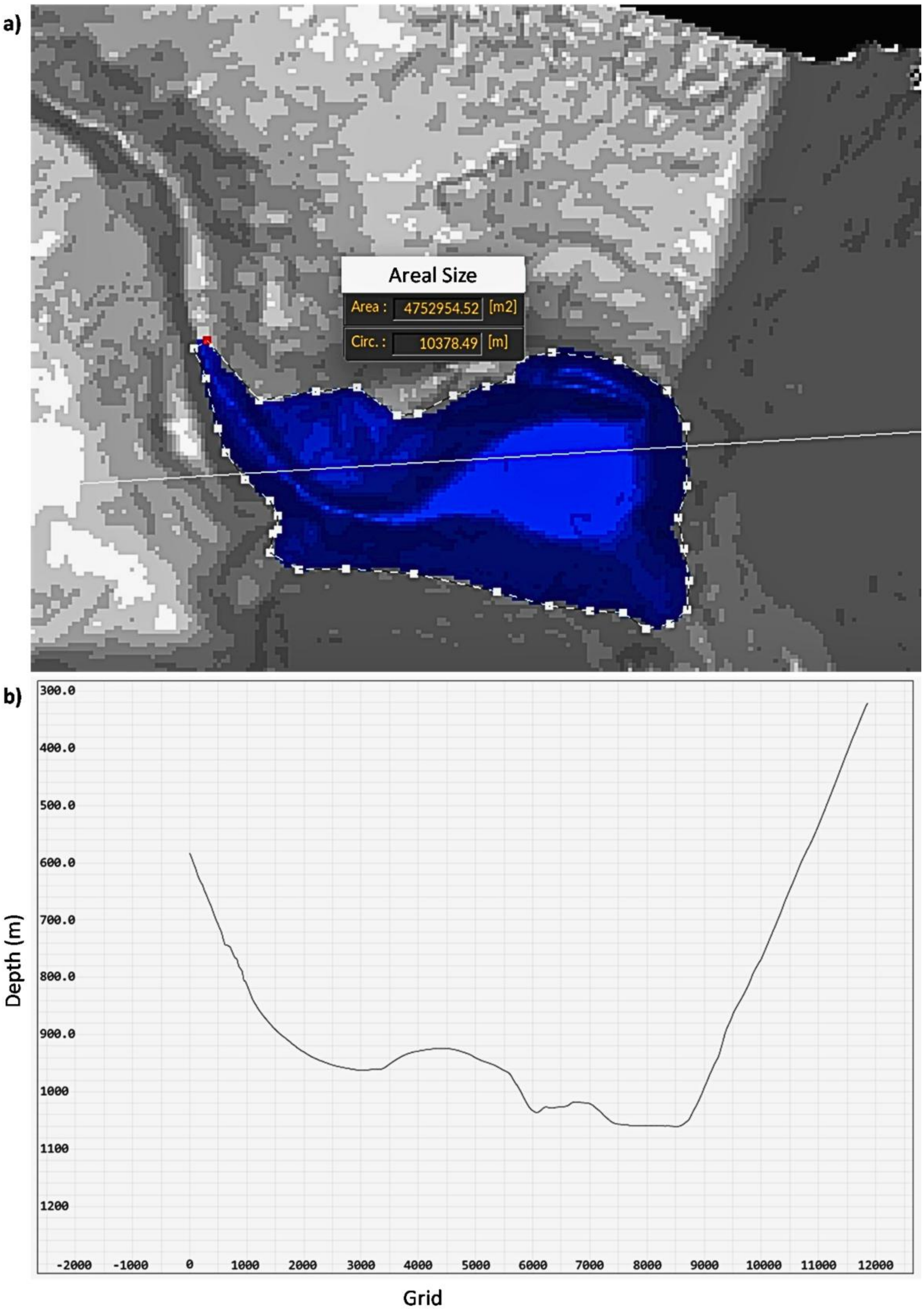

Figure 7. (a) Areal Size of Pantar Strait with a Depth of More Than 1,000 m. The White Line Denotes the Cross-Section of Bathymetry in (b). (b) Cross-Section of Bathymetry as Shown by the White Line in (a) and the Red Dashed Line in Figure 3b.

3.2. Vertical Profile of Temperature

The vertical distribution of temperature obtained from CTD measurement demonstrates that below 400 m, the temperature is lower than 10 °C. However, we can see that the 10 °C isotherm at 8.425 °S to 8.35 °S is shallower than that at 8.35 °S to 8.3 °S, indicating a shallow mixed layer depth in the southern part Figure 8. This may be due to differences in tidal conditions during CTD casting. CTD casting at stations 2 and 3 (4 and 5) was conducted during the ebb (flood) tide Figure 2. Shoaling at mixed layer depths is often associated with mechanisms such as tidal mixing and the dynamics of ocean currents. For instance, in regions where tidal forces are strong, such as off the Yangtze River Estuary, tidal mixing can induce upwelling by creating horizontal density gradients across tidal fronts. This occurs as part of a secondary circulation driven by cross-frontal density gradients, with topographic features playing a significant role in directing bottom currents upwards, thereby regulating the location and intensity of tidal fronts (Lü *et al.,* 2006). In the case of the Pantar Strait, shoaling mixed-layer depths during flood tides also indicate an upwelling signal. The upwelling process in the Pantar Strait reduced the temperature of the surface layer. Thus, tides also influence variations in the surface temperature along the Pantar Strait. Nevertheless, the surface temperature drop is not comparable with the case of EUE at the Mulut Kumbang Strait as reported by Wirasatriya *et al.,* (2023), which can reduce surface temperature by ~10 °C.

A straightforward calculation can be employed to illustrate the propagation of cold-water masses from the deepest basin of the southern Pantar Strait to the Mulut Kumbang Strait during Easterly Upwelling Events (EUE). As shown in Figure 8a, the deepest point in the southern Pantar Strait reached a maximum depth of 1,060 m, whereas the horizontal distance separating this basin from the Mulut Kumbang Strait is approximately 19,425 m. Consequently, the diagonal distance accounting for both depth and horizontal displacement was calculated to be 19,454 m. Simulations conducted by Prasetyo *et al.* (2024) indicate that the maximum current velocity in the Pantar Strait during the spring tide varies between 2.8 m/s and 3.2 m/s. Using an average current velocity of 3 m/s, the cold water mass required roughly 1.8 h to traverse the diagonal distance from the deepest basin to the Mulut Kumbang Strait. This estimated duration aligns well with the observed EUEs, which typically last between 1 and 2 h (Wirasatriya *et al.,* 2023, 2025a).

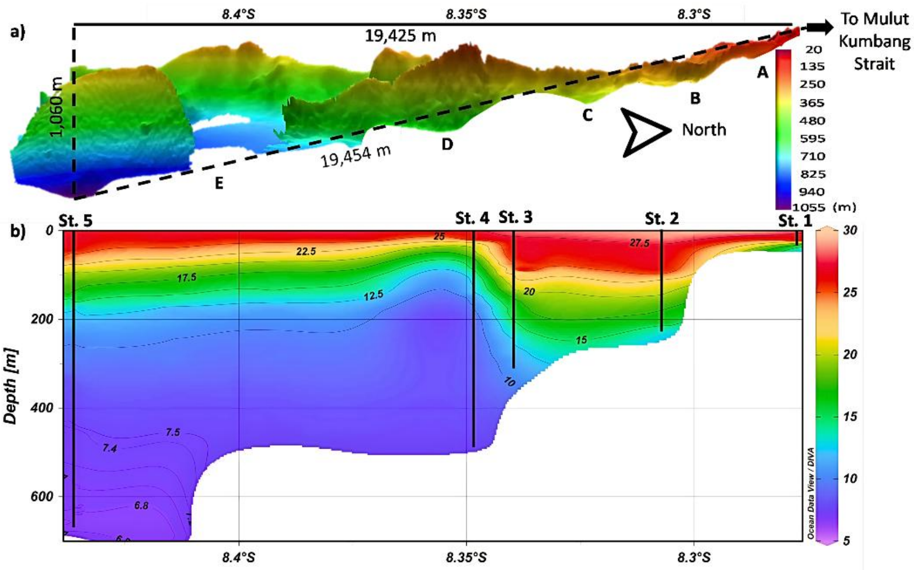

Figure 8. Side View of Bathymetry of Pantar Strait with the Position of Basins A, B, D, and E. (b) Vertical Distribution of Temperatures Interpolated from CTD Measurement.

3.3. Discussion

Using an MBES, we revealed the complex bottom topography of the southern Pantar Strait, providing new evidence for the cold water source of the EUE in the Mulut Kumbang Strait. Previously, the limitation in bathymetric coverage from SBES observations, as reported by Wirasatriya *et al.* (2023), identified only a single basin (Basin B) between Pura Island and the southwestern Alor subdistrict, which they posited as the source of the cold-water mass of the EUE. However, the more detailed bathymetric survey presented in this study revealed five distinct basins aligned along the channel, indicating a far more intricate bathymetric architecture than previously recognized. This complexity likely plays a crucial role in modulating cold-water mass dynamics by providing a pathway that influences water mass flow and mixing. Furthermore, while Astuti *et al.* (2025) proposed that the Savu Sea is the source of the cold-water mass, the deeper bathymetry in Basin E provides compelling evidence that the cold-water mass could have originated within the Pantar Strait. Their indication was based on the genetic material of bathypelagic fish obtained during the EUE in the Mulut Kumbang Strait. Because bathypelagic fishes live at a depth of 1,000–4000 m depth, the source of the cold-water mass during EUE should come from a water column deeper than 1,000 m. Based on the bathymetry map by Setiawan *et al.* (2020), the maximum depth of the Pantar Strait is less than 1,000 m. Thus, Astuti *et al.* (2025) assumed that the source of the cold-water mass came from the Savu Sea, which has a maximum depth of 3470 m (Kartaadiputra *et al.,* 1982; Van Der Werff, 1995).

The new bathymetry presented in this study provides an alternative hypothesis that the source of the cold-water mass of EUE may come from the southernmost basin of the Pantar Strait, that is

Basin E. Thus, the genetic material of bathypelagic fishes, that is Benthosema fibulatum, Dasyscopelus asper, Diaphus garmani, Diaphus suborbitalis, Diaphus watasei, and Howella cf. broidei obtained by Astuti *et al.* (2025) during EUE in the Mulut Kumbang Strait may come from Basin E, which has an area deeper than 1,000 m.

The finding of a tapered channel from Basin E to the Mulut Kumbang Strait exemplifies how channel geometry and bathymetry control tidal current acceleration and the associated upwelling phenomena. Narrow channels and sills have long been recognized as amplifying tidal currents, often generating localized internal mixing and secondary circulation that leads to upwelling along strait boundaries (Tassigny *et al.,* 2026; Nakamura *et al.,* 2000). In this context, flood tide advection into the strait brings subsurface cold, nutrient-rich water masses into shallower zones, while ebb tides flush these waters back into the open sea, producing a highly dynamic exchange driven by the tidal cycle (Kawaguchi *et al.,* 2020).

Moreover, frictional effects on the seafloor during strong tidal currents, especially under spring tide conditions, can generate bottom Ekman transport and vertical motion, which contribute to upwelling. These bottom boundary layer dynamics are critical in straits with complex bathymetry, where the interaction of tidal currents with seafloor topography induces secondary circulation that is responsible for the vertical displacement of colder waters (Kawaguchi *et al.,* 2020; Lieberthal *et al.,* 2019). The repeated twice-daily pattern of upwelling events is in accordance with the semidiurnal tidal constituents commonly observed in narrow straits, where two flood and two ebb phases occur within each tidal day (Longhitano, 2010; Tsimplis *et al.,* 1995).

Despite the relatively small tidal amplitude, tidal upwelling in similar microtidal or semi-closed basins can produce significant local enhancements in mixing and vertical nutrient transport, as tidal currents are spatially intensified through geometric contraction or resonance effects. These mechanisms explain the upwelling strictly confined to the Mulut Kumbang Strait, as opposed to a broader coastal setting where wind forcing dominates (Longhitano *et al.,* 2010). This phenomenon starkly contrasts broad coastal upwelling systems, where wind forcing predominantly drives vertical transport. The distinct confinement of upwelling to the Mulut Kumbang Strait indicates that tidal dynamics, rather than wind forcing, are the principal drivers at this location, aligning with numerical simulations of tidal upwelling in narrow channels (Lin & Gan, 2024; Kim *et al.,* 2023).

Although the present study provides an initial transport estimate, this simplified approach neglects the multivariate complexity of hydrodynamics, such as the effects of irregular bottom topography, vertical stratification, and internal wave interactions, which critically modulate cold-water propagation. Topographic features can induce localized tidal amplification, internal tide generation, flow separation, and mixing (Cucco *et al.,* 2016; Bignami *et al.,* 2025), whereas density stratification mediates internal wave dynamics and density-driven flows that influence water mass transformation and pathways (Evans *et al.,* 2018; Li *et al.,* 2020). These processes emphasize the need for further high-resolution hydrodynamic and numerical modelling to fully characterize cold-water transport mechanisms in this complex strait system.

Overall, the evidence indicates that the phenomenon in the Mulut Kumbang Strait is a distinctive tide-driven upwelling system that is cyclical in nature and is controlled by the interaction of spring tide dynamics with a narrow channel morphology. The fortnightly spring neap tidal variations regulate the timing and intensity, while the narrow geometry concentrates tidal currents sufficiently strongly to produce the observed cold-water ingress during flood tides and egress during ebb tides. Such tidal upwelling not only alters local thermal and nutrient conditions but can also have broader ecological impacts on productivity and biogeochemical cycling in the strait and adjacent waters (Susanto and Ray, 2022; Sharples, 2007).

In summary, integrating recent bathymetric and ecological data with established tidal dynamics frameworks highlights that tide-generated upwelling in narrow straits, such as Mulut Kumbang, arises from the amplification of semidiurnal tidal currents constrained by channel geometry. Spring neap tidal modulation imparts fortnightly variability, while bottom boundary layer processes foster vertical cold-water flux. The cyclic import and export of nutrient-rich cold water establishes a unique upwelling system with significant implications for regional oceanography and marine ecosystems, consistent with theoretical and observational insights into global strait-induced upwelling phenomena (Lin & Gan, 2024; Bignami *et al.,* 2025; Kawaguchi *et al.,* 2020).

Future research should focus on investigating the dynamics of cold-water mass propagation through a tapered channel connecting the basins to the Mulut Kumbang Strait. High-resolution temporal monitoring of temperature and salinity profiles along the channel during the EUE could provide insights into how cold-water masses are transported during EUEs. Additionally, numeri cal modeling of the hydrodynamics in this region would help simulate the flow patterns and confirm the role of the channel in directing the cold-water mass. Realistic simulations require a three-dimensional baroclinic numerical model that incorporates detailed bathymetric data obtained from MBESs. Such modeling approaches capture nonlinear interactions between topography, stratification, tidal currents, and other forcing mechanisms, enabling a more accurate depiction of cold-water mass propagation during EUE. The significance of including such physical complexities in numerical studies has been well illustrated for the Southern Ocean and other straits, where three-dimensional coupled models reveal processes that are overlooked in simplified flow calculations (Evans *et al.,* 2018; Cucco *et al.,* 2016; Wells *et al.,* 2025). Understanding this modeling task will provide a comprehensive understanding of water mass dynamics in the southern Pantar Strait. Furthermore, the tapered shape of the channel that connects the five basins to the Mulut Kumbang Strait likely concentrates and accelerates the flow of the cold-water mass, creating a funneling effect that enhances upwelling during extreme events. Further investigation of the hydrodynamics of this channel is essential to understand how its shape affects the propagation of cold water and contributes to the intensity of upwelling events. Because the cold-water mass could be periodically funneled toward the Mulut Kumbang Strait during specific tidal conditions, this potentially explains the timing and recurrence of EUEs. Thus, future studies should examine the correlation between the timing of spring tides, availability of cold water in the basins, and frequency of EUE to better understand the factors controlling these events.

4. Conclusion

Using a MBES, we were able to identify five basins (A–E) in the southern Pantar Strait that may act as source reservoirs and pathways for the cold-water mass associated with the EUE in the Mulut Kumbang Strait. Basin A is located south of the Mulut Kumbang Strait at a depth of ~150 m. Basins B, C, and D lie to the south at depths of ~350, ~400, and ~600 m, respectively. The deepest basin is Basin E, which is bordered by the Savu Sea has a maximum depth of 1,060 m. While all five basins are potential sources of cold-water masses, Basin E, located in the southernmost part of the Pantar Strait, is particularly significant because of its depth, which has a 4.75 km^2 area of 1,000 m or deeper. The cold-water mass is hypothesized to originate from this basin because the temperature data from CTD measurements confirm that water below 400 m is colder than 10 °C, supporting the idea that deep cold water is funneled through the tapered channel. In the future, the direct validation of cold-water propagation will require current measurements (e.g., ADCP/moorings) during spring tides or 3D baroclinic modeling using this new bathymetry.

Acknowledgements

We would like to thank the Indonesian Navy Hydrography and Oceanography Center (PUSHIDROSAL) for organizing the Jala Citra Expedition 3 - 2023 “Flores”. In this research, data acquisition and preprocessing were supported by KRI Spica-934 as the research vehicle. Special thanks to UPTD Pengelola Taman Perairan Kepulauan Alor dan Laut Sekitarnya for the research permit and Mr. Rachmad Marweki and his family for their hospitality in providing the accommodation during the field survey.

Author Contributions

Conceptualization: Wirasatriya, A., Harsono, G., Susanto, R. D., Nugroho, D.; **methodology**: Wirasatriya, A., Harsono, G., Putranto, R. T., Pratama, D. J., Medhika, Y. T.; **investigation**: Wirasatriya, A., Hamzah, F., Triyulianti, I., Elake, A. Y., Setiabudi, G. I., Khair, D. R., Syafaat, M., Pratama, D. J., Medhika, Y. T., Sasongko, A. S.; **writing—original draft preparation**: Wirasatriya, A., Susanto, R. D., Cahyani, N. K. D.; **writing—review and editing**: Wirasatriya, A., Harsono, G., Haryanti, D., Maslukah, L., Wijaya, Y. J., Rifai, A., Maro, J.F; **visualization**: Putranto, R. T., Widiyandono, R. T., Helmi, M., Medhika, Y. T., Darminto.. All authors have read and agreed to the published version of the manuscript.

Conflict of interest

All authors declare that they have no conflicts of interest.

Data availability

Data is available upon Request.

Funding

This research is funded by Diponegoro University through World Class Research University scheme with contract number: 222-737/UN7.D2/PP/IV/2025. This work is also supported by the Physical Oceanography program of the National Science Foundation (NSF; grant #2242151) through the University of Maryland for R. Dwi Susanto.

References

Astuti, Y. D., Nursalim, N., Al Malik, M. D., Syakal, E. R., Maslukah, L., Wijaya, Y. J., Putranto, R. T., Krisna, H. N., Mustaqim, I., Susanti, A. F. S., Susanto, R. D., Cahyani, N. K. D., & Wirasatriya, A. (2025). Unveiling deep-sea fish communities through eDNA analysis during extreme upwelling events in Pantar Strait, Indonesia. *Regional Studies in Marine Science*, 91, 104536. doi: 10.1016/j.rsma.2025.104536

Bignami, F., Alpers, W., Cavaliere, D., La Forgia, G., & Sannino, G. (2025). Observations and generation of internal waves in the Strait of Sicily. *Continental Shelf Research*, 284, 105349. doi: 10.1016/j.csr.2024.105349

Canadian Hydrographic Service .(2012). *CUBE Bathymetric data Processing and Analysis.* Retrieved From https://charts.gc.ca/documents/data-gestion/bathymetric-traitement/bathymetric-traitement-eng.pdf

Chen, G., Li, Y., Han, W., & Wang, D. (2016). Interannual Variability of Equatorial Eastern Indian Ocean Upwelling: Local versus Remote Forcing. *Journal of Physical Oceanography,* 46(3), 789–807. doi: 10.1175/jpo-d-15-0117.1

Cucco, A., Sinerchia, M., Fazioli, L., Olita, A., Ribotti, A., Quattrocchi, G., Sorgente, R., & Tedesco, C. (2016). Hydrodynamic modelling of coastal seas: the role of tidal dynamics in the Messina Strait, Western Mediterranean Sea. *Natural Hazards and Earth System Sciences,* 16(7), 1553–1569. doi: 10.5194/nhess-16-1553-2016

Delman, A. S., Mcclean, J. L., Talley, L. D., & Sprintall, J. (2016). Anomalous Java cooling at the initiation of positive Indian Ocean Dipole events. *Journal of Geophysical Research: Oceans*, 121(8): 5805–5824. doi: 10.1002/2016jc011635

Du, Y., Qu, T., & Meyers, G. (2008). Interannual Variability of Sea Surface Temperature off Java and Sumatra in a Global GCM*. *Journal of Climate,* 21(11): 2451–2465. doi: 10.1175/2007jcli1753.1

Evans, D. G., Naveira Garabato, A. C., Zika, J. D., & Nurser, A. J. G. (2018). The Cold Transit of Southern Ocean Upwelling. *Geophysical Research Letters,* 45(24). doi: 10.1029/2018gl079986

García-Reyes, M., & Largier, J. (2010). Observations of increased wind-driven coastal upwelling off central California. *Journal of Geophysical Research: Oceans,* 115(C4). doi: 10.1029/2009jc005576

Harvey, J. B. J., Ryan, J. P., & Zhang, Y. (2021). Influences of extreme upwelling on a coastal retention zone. *Frontiers in Marine Science,* 8, 648944. doi: 10.3389/fmars.2021.648944

Kämpf, J. (2015). On the majestic seasonal upwelling system of the Arafura Sea. *Journal of Geophysical Research: Oceans*, 121, 1218–1228. doi: 10.1002/2015JC011197

Kämpf, J., & Chapman, P. (2016). The functioning of coastal upwelling systems. *In Upwelling Systems of the World,* 31–65. doi: 10.1007/978-3-319-42524-5_2

Kartaadiputra, L. W., Ahmad, Z., & Reymond, A. (1982). Deep sea basins in Indonesia. *In Proceedings of the Indonesian Petroleum Association 11th Annual Convention,* 53–81.

Kawaguchi, Y., Nishioka, J., Nishino, S., Fujio, S., Lee, K., Fujiwara, A., Yanagimoto, D., Mitsudera, H., & Yasuda, I. (2020). Cold Water Upwelling Near the Anadyr Strait: Observations and Simulations. *Journal of Geophysical Research: Oceans*, 125(9). doi: 10.1029/2020jc016238

Khomsin, K., Pratomo, D. G., & Saputro, I. (2021). Comparative analysis of singlebeam and multibeam echosounder bathymetric data. *IOP Conference Series: Materials Science and Engineering,* 1052, 012015. doi: 10.1088/1757-899X/1052/1/012015

Kim, D., Choi, J.-G., Park, J., Kwon, J.-I., Kim, M.-H., & Jo, Y.-H. (2023). Upwelling processes driven by contributions from wind and current in the Southwest East Sea (Japan Sea). *Frontiers in Marine Science*, 10, 1165366. doi: 10.3389/fmars.2023.1165366

Li, Y., Curchitser, E. N., Wang, J., & Peng, S. (2020). Tidal Effects on the Surface Water Cooling Northeast of Hainan Island, South China Sea. *Journal of Geophysical Research: Oceans,* 125(10). doi: 10.1029/2019jc016016

Lin, S., & Gan, J. (2024). Dynamics of tidal effects on coastal upwelling circulation over variable shelves in the northern South China Sea. *Journal of Geophysical Research: Oceans*, 129(9), e2024JC021193. doi: 10.1029/2024JC021193

Lieberthal, B., Huguenard, K., Ross, L., & Bears, K. (2019). The Generation of Overtides in Flow Around a Headland in a Low Inflow Estuary. *Journal of Geophysical Research: Oceans*, 124(2), 955–980. doi: 10.1029/2018jc014039

Longhitano, S. G. (2010). The record of tidal cycles in mixed silici–bioclastic deposits: examples from small Plio–Pleistocene peripheral basins of the microtidal Central Mediterranean Sea. *Sedimentology*, 58(3), 691–719. doi: 10.1111/j.1365-3091.2010.01179.x

Longhitano, S. G., Sabato, L., Tropeano, M., & Gallicchio, S. (2010). A Mixed Bioclastic-Siliciclastic Flood-Tidal Delta in a Micro Tidal Setting: Depositional Architectures and Hierarchical Internal Organization (Pliocene, Southern Apennine, Italy). *Journal of Sedimentary Research*, 80(1), 36–53. doi: 10.2110/jsr.2010.004

Lü, X., Yuan, Y., Xia, C., Qiao, F., & Zhu, J. (2006). Upwelling off Yangtze River estuary in summer. *Journal of Geophysical Research: Oceans,* 111(C11). doi: 10.1029/2005jc003250

Moore II, T. S., Marra, J., & Alkatiri, A. (2003). Response of the Banda Sea to the southeast monsoon. *Marine Ecology Progress Series, 261*, 41–49.

Nakamura, T., Awaji, T., Hatayama, T., Akitomo, K., & Takizawa, T. (2000). Tidal Exchange through the Kuril Straits. *Journal of Physical Oceanography*, 30(7), 1622–1644. doi: 10.1175/1520-0485(2000)030<1622:tettks>2.0.co;2

Narayan, N., Mulitza, S., Paul, A., & Schulz, M. (2010). Trends in coastal upwelling intensity during the late 20th century. *Ocean Science,* 6(3), 815–823. doi: 10.5194/os-6-815-2010

Ningsih, N. S., Rakhmaputeri, N., & Harto, A. B. (2013). Upwelling variability along the southern coast of Bali and in Nusa Tenggara waters. *Ocean Science Journal,* 48(1), 49–57. doi: 10.1007/s12601-013-0004-3

Prasetyo, A. T., Patriadi, A., Ahsin, A., Nurhidayat, N., Purwanto, B., Sobaruddin, D. P., Muslim, M., Hendri, M., Hermialingga, S., & Kurniasih, E. M. (2024). Safety Assessment of Ocean Current in Pantar Strait for Marine Tourism. ILMU KELAUTAN: Indonesian *Journal of Marine Sciences,* 29 (4), 530-542. doi:10.14710/ik.ijms.29.4.530-542

Putranto, R. T., Wirasatriya, A., Rahmadani, M. A., Iriani, R. N., Mustaqim, I., Susanti, A. F. S., Putri, S. A., Ginanjar, S., Adiningsih, S., Wijaya, Y. J., Susanto, R. D., Sugianto, D. N., & Widowati, L. L. (2025). Internet of Things-based monitoring system on the extreme upwelling event in the seas of Alor Kecil, Alor Island, Indonesia. The *Journal of Ocean Technology,* 20(3), 80–100. doi: 10.48336/by4b-yn62

Reynaud, J.-Y., & Dalrymple, R. W. (2011). Shallow-Marine Tidal Deposits. *Springer Netherlands*, 335-369. doi: 10.1007/978-94-007-0123-6_13

Saraswat, R., Mackensen, A., Nigam, R., Naidu, P. D., & Weldeab, S. (2005). A first look at past sea surface temperatures in the equatorial Indian Ocean from Mg/Ca in foraminifera. Geophysical Research Letters, 32(24) doi: 10.1029/2005gl024093

Sharples, J. (2007). Potential impacts of the spring-neap tidal cycle on shelf sea primary production. *Journal of Plankton Research*, 30(2), 183–197. doi: 10.1093/plankt/fbm088

Setiawan, R. Y., & Habibi, A. (2011). Satellite detection of summer chlorophyll-a bloom in the Gulf of Tomini. *IEEE Journal of Selected Topics in Applied Earth Observations and Remote Sensing*, 4(4), 944–948. doi: 10.1109/JSTARS.2011.2163926

Setiawan, R. Y., & Kawamura, H. (2011). Summertime phytoplankton bloom in the south Sulawesi Sea. IEEE Journal of Selected Topics in Applied Earth Observations and Remote Sensing, 4(1), 241–244. https://doi.org/10.1109/JSTARS.2010.2094604

Setiawan, R. Y., Setyobudi, E., Wirasatriya, A., Muttaqin, A. S., & Maslukah, L. (2019). The influence of seasonal and interannual variability on surface chlorophyll-a off the Western Lesser Sunda Islands. *IEEE Journal of Selected Topics in Applied Earth Observations and Remote Sensing,* 12(11), 4191–4197. doi: 10.1109/JSTARS.2019.2948385

Setiawan, R. Y., Wirasatriya, A., Hernawan, U., Leung, S., & Iskandar, I. (2020). Spatio-temporal variability of surface chlorophyll-a in the Halmahera Sea and its relation to ENSO and the Indian Ocean Dipole. *International Journal of Remote Sensing,* 41(1), 284–299. doi: 10.1080/01431161.2019.1641244

Susanto, R. D., Moore II, T., & Marra, J. (2006). Ocean color variability in the Indonesian Seas during the SeaWiFS era. *Geochemistry Geophysics Geosystems,* 7(5), 1–16. doi: 10.1029/2005GC001009

Susanto, R. D., & Ray, R. D. (2022). Seasonal and Interannual Variability of Tidal Mixing Signatures in Indonesian Seas from High-Resolution Sea Surface Temperature. *Remote Sensing*, 14(8), 1934. doi:10.3390/rs14081934

Sie, F.M.P., Yasunaka, S. & Wirasatriya, A. (2025) Seasonal and interannual variations in local minimum sea surface temperature and maximum chlorophyll-a around the Savu Sea, Indonesia. Progress in Earth and Planetary Sciene 12(106). doi: 10.1186/s40645-025-00781-9

Tassigny, A., Bardoel, S. L., Valran, T., Viboud, S., Gostiaux, L., Sommeria, J., Bordois, L., Carton, X., & Negretti, M. E. (2026). A realistic physical model of the Gibraltar Strait. *Ocean Science*, *22*(1), 459–500. doi: 10.5194/os-22-459-2026

Tsimplis, M. N., Proctor, R., & Flather, R. A. (1995). A two-dimensional tidal model for the Mediterranean Sea. *Journal of Geophysical Research: Oceans*, *100*(C8), 16223–16239. doi: 10.1029/95jc01671

Van Der Werff, W. (1995). Cenozoic evolution of the Savu Basin, Indonesia: Forearc basin response to arc-continent collision. Marine and Petroleum Geology, 12(3), 247–262. doi: 10.1016/0264-8172(95)98378-I

Wang, D., Zhuang, W., Xie, S.-P., Hu, J., Shu, Y., & Wu, R. (2012). Coastal upwelling in summer 2000 in the northeastern South China Sea. Journal of Geophysical Research: Oceans, 117(4), Article C04009. doi: 10.1029/2011JC007465

Weingartner, T. J., & Weisberg, R. H. (1991). A Description of the Annual Cycle in Sea Surface Temperature and Upper Ocean Heat in the Equatorial Atlantic. Journal of Physical Oceanography 21(1) : 83–96. doi: 10.1175/1520-0485(1991)021<0083:adotac>2.0.co;2

Wells, C., Pringle, J., & Stretch, D. (2025). Refining the role of bathymetry, hydrodynamics and upwelling at various scales along the coral reefs at Sodwana Bay, South Africa. *Ocean Dynamics*, 75(1), 13. doi: 10.1007/s10236-024-01646-3

Wirasatriya, A., Basana, A. M., Indrayanti, E., Suryoputro, A. A. D., Susanto, R. D., Hartati, R., Taufiq-SPJ, N., Maro, J. F., Wetchayont, P., Putra, M. I. H., & Sahri, A. (2025a). Increasing dolphin occurrences during extreme upwelling events: Potential nonharmful and sustainable marine wildlife tourism at Mulut Kumbang Strait, Alor Kecil Village, Alor Island, Indonesia. *Progress in Oceanography*, 240, 103613. doi: 10.1016/j.pocean.2025.103613

Wirasatriya, A., Iryanthony, S. B., Susanto, R. D., Agustiadi, T., Kunarso, Ismanto, A., Helmi, M., Zainuri, M., Widiaratih, R., Harsono, G., Nugroho, D., Purwandana, A., Fitria, S., Maro, J. F., Kitarake, Y. N. S., Dollu, E. A., Widiyandono, R. T., Qiu, C., Sakti, A. D., … Kelendonu, E. (2025b). Spatial distribution of extreme upwelling event in the seas of Alor Kecil, Indonesia, revealed by UAV's thermal infrared sensor. *Regional Studies in Marine Science*, 90, 104451. doi: 10.1016/j.rsma.2025.104451

Wirasatriya, A., Setiawan, J. D., Sugianto, D. N., Rosyadi, I. A., Haryadi, H., Winarso, G., Setiawan, R. Y., & Susanto, R. D. (2020). Ekman dynamics variability along the southern coast of Java revealed by satellite data. International *Journal of Remote Sensing*, 41(21), 8475–8496. doi: 10.1080/01431161.2020.1797215

Wirasatriya, A., Sugianto, D. N., Helmi, M., Maslukah, L., Widiyandono, R. T., Herawati, V. E., Subardjo, P., Handoyo, G., Haryadi, Marwoto, J., Suryoputro, A. A. D., Atmodjo, W., & Setiyono, H. (2019a). Heat flux aspects on the seasonal variability of sea surface temperature in the Java Sea. *Ecology, Environment and Conservation*, 2(1), 434–442.

Wirasatriya, A., Sugianto, D. N., Helmi, M., Setiawan, R. Y., & Koch, M. (2019b). Distinct characteristics of SST variabilities in the Sulawesi Sea and the northern part of the Maluku Sea during the southeast monsoon. *IEEE Journal of Selected Topics in Applied Earth Observations and Remote Sensing*, 12(6), 1763–1770.

Wirasatriya, A., Susanto, R. D., Kunarso, K., Jalil, A. R., Ramdani, F., & Puryajati, A. D. (2021). Northwest monsoon upwelling within the Indonesian seas. *International Journal of Remote Sensing*, 42(14), 5437–5458. doi: 10.1080/01431161.2021.1918790

Wirasatriya, A., Susanto, R. D., Setiawan, J. D., Agustiadi, T., Iskandar, I., Ismanto, A., Nugraha, A. L., Puryajati, A. D., Kunarso, Purwandana, A., Ramdani, F., Lestari, T. A., Maro, J. F., Kitarake, Y. N. S., Sailana, Y. L., Goro, M. S., Hidayah, B. K., Widiaratih, R., Fitria, S., & Dollu, E. A. (2023). Extreme upwelling events in the seas of the Alor Kecil, Alor Island, Indonesia. *Oceanography*, 36(1), 3–0. doi: 10.5670/oceanog.2023.107

Xing, Q., Yu, H., Yu, H., Wang, H., Ito, S.-I., & Yuan, C. (2021). Evaluating the Spring-Neap Tidal Effects on Chlorophyll-a Variations Based on the Geostationary Satellite. *Frontiers in Marine Science*, 8. doi: 10.3389/fmars.2021.758538